Ebaid and Ammari *Renewables (2015)2:19*
DOI 10.1186/s40807-015-0017-x

Renewables:
Wind, Water, and Solar
a SpringerOpen Journal

ORIGINAL RESEARCH

Open Access

Modeling and analysis of unsteady-state thermal performance of a single-slope tilted solar still

Munzer S. Y. Ebaid[1*] and Handri Ammari[2]

Abstract

Jordan lies in high solar insolation band and the vast solar potential can be exploited to convert saline water to potable water. The most economical and easy way to accomplish this objective is using solar still. Modeling and performance analysis of a single slope tilted solar still were investigated in this paper A computer simulation of the still is carried out to examine and predict its unsteady-state thermal performance. Runge–Kutta method of the fifth order was used to solve the developed partial differential equations numerically for the theoretical model of the solar still, and with the transient effects accounted for. Prediction of the time-dependent temperature distribution along the absorber plate for the brine water, the absorber, and glass cover was achieved. The thermal efficiency of the solar still over a day was predicted at different operating conditions (Solar input, ambient temperature, dust and wind velocity). The results of the simulation mathematical model were validated by comparison with experimental data obtained from an experimental tilted solar still system that has been built for comparison purposes. The performance of both systems, theoretical and experimental, is assessed under the same conditions. Numerical and experimental results showed reasonable agreement, and the best performance was obtained at flow rate of $\dot{m}$ of 0.348 kg/h for both the experimental and numerical results. Also, the work indicates that the theoretical model can be employed in the design of solar stills.

Keywords: Solar energy, Tilted solar still, Water distillation, Mathematical model

Background

The demand for fresh water has been on the rise due to population explosion and rapid industrial growth all over the world, whereas the availability of drinking water is decreasing day by day. To overcome this problem there is a need for some sustainable source for water distillation. However, economic considerations may render conventional distillation of brackish or saline waters that may be found in deserts and sea shores, respectively. Therefore, solar energy, despite being a much lower grade energy source than electric power or fossil fuel, would be a potential option for distillation through using stills in such places. Duffie and Beckman (1991) reported that for places whereby plenty of solar energy is available and the demand for fresh water to provide hygienic potable water is not too large, solar still would be an ideal solution for a single house or a small community. The application of solar energy to domestic water distillation is highly feasible in Jordan, due to the annual daily average solar irradiance in Jordan ranges between 5 and 7 kWh/m^2 (NASA Surface Meteorology and Solar Energy 2015) which is about 40 % higher than many regions of Europe and most of North America. The rate of penetration of solar systems is expected to increase during the coming years, resulting in a considerable decrease in environmental pollution.

There are several types of solar distillation stills that have been devised for converting available brackish or waste water into potable water. The horizontal basin-type still is one of these. And because of its low productivity, it is not commonly used. On the other hand, tilted

*Correspondence: mebaid2@philadelphia.edu.jo
[1] Mechanical Engineering Department, Philadelphia University, Amman, Jordan
Full list of author information is available at the end of the article

solar stills heat up more rapidly, operate at higher mean temperatures, have lower thermal capacity, and produce somewhat more potable water. There are also other types of solar stills that have been evolved, such as multistage flash distillation stills and solar concentrator stills. Previous work on solar stills by researchers in the open literature is divided into two sections: experimental and numerical as described hereafter.

Experimental work

Solar stills have been thoroughly studied experimentally to improve the productivity of all types of solar stills, whether passive or active systems. Some researchers, (Tiwari et al. 2003; Murugavela et al. 2008; Kaushal 2010; Kabeel and El-Agouz 2011; Velmurugana and Srithar 2011; Sampathkumar et al. 2010; Xiao et al. 2013), have reviewed the studies and developments of research work on both passive and active solar still distillation systems. The basin-type solar stills are the most frequently studied over the years by researchers of solar distillation systems. Their investigations have been directed towards improving the daily distillate output per unit basin area of solar still (Naim and Abd El Kwui 2002; Abu-Hijleh and Rababah 2003; Al-Hayeka and Badran 2004; Badran and Al-Tahaineh 2005; Tiwari and Tiwari 2006; Sahoo et al. 2008; Abdallah et al. 2009). Various techniques to enhance the yield of distilled water from tilted solar stills have been experimented and presented by many researchers, for example, a tilted double-sided solar still (St. Headley 1973), an inverted trickle solar still (Badran et al. 2004), and tilted wick solar still (Tripathi and Tiwari 2004) and (Tanaka and Nakatake 2007). Recently, different designs of solar stills were proposed and investigated by researchers. Among them, the design of basin type double solar still (Murugaval and Srithar 2011), a weir type cascade solar still (Tabiriz et al. 2010), an integrated basin solar still with a sandy heat reservoir (Tabiriz and Sharak 2010), a tubular type (Ahsan et al. 2012), a wick type solar still (Mahdi et al. 2011), and finally a conventional single sloped solar still and a modified stepped solar still (Kabeel et al. 2012).

Numerical work

To ensure high quality and satisfactory performance of solar still systems, computer simulations are being used to optimize the design of a typical system. Many researchers, therefore, performed theoretical and numerical analysis of solar stills. Fath and Hosney (2002) presented a theoretical study of the thermal performance of a single-sloped basin still with enhanced evaporation and a built-in additional condenser. Abu-Arabi et al. (2002) modeled a solar still with cooling water flowing between a double-glass cover, and found that the effects of the cooling water flow rate and the glass spacing on productivity were small. Voropoulos et al. (2003) developed an analytical simulation method of energy behavior of solar stills, where the main climatic data and operating conditions of the still with distilled water output on day and night base were related to linear equations using characteristic coefficients determined by experiments.

Additional numerical works on passive and active solar stills for different Indian climatic conditions were carried out by Singh and Tiwari (2004). Their results showed that the annual yield mainly depends on water depth, inclination of condensing cover, and the collector for both passive and active solar stills. Janarthanan et al. (2005) derived an analytical expression for the thermal efficiency of evaporative heat loss and heat transfer for open- and closed-cycle systems of floating tilted wick solar stills in terms of system design and climatic parameters. Shukla and Sorayan (2005) derived expressions for water and glass temperatures, yield, and efficiency of both single- and double-slope multi-wick solar distillation systems in quasi-steady state conditions. Tiwari and Tiwari (2007) conducted a seasonal performance analysis for six different water depths in a single-slope passive solar still of cover inclination of 30°. They found that the lower water depth gave the highest annual yield. They also developed a thermal model that validated the hourly yield for various water depths in summer and winter.

Khalifa and Hamood (2009) derived four correlations to illustrate the effect of solar radiation, dyes, cover slope, and brine depth on the productivity of the basin type solar still. The correlations developed showed that the solar still productivity could be influenced by the brine depth alone up to 33 %, and by the tilt angle alone up to 63 %. The still productivity could be enhanced by adding dark soluble dye to the brine by up to 20 %. Tanaka and Nakatake (2009) presented a theoretical analysis of a tilted-wick solar still with an inclined flat plate external reflector on a winter solstice day at 30°N latitude. Their results showed that the daily amount of the distillate of a still with an inclined reflector would be about 15 or 27 % greater than that with a vertical reflector when the reflector's length is half of or the same as the still's length. Madholpa and Johnstone (2009) carried out a numerical study of a passive solar still with separate condenser. They reported that the theoretical productivity was 62 % higher than that of the conventional still.

Some researchers claimed that the performance of solar still can be improved using a hybrid photovoltaic/thermal (PV/T) system (Dev and Tiwari 2010; Kumar et al. 2010). In addition, Velmurugan and Srithar (2011) carried out an extensive review of numerical as well as experimental investigations on basic types of solar still. Ahsan et al. (2013) presented a detailed comparison of

several numerical models for the estimation of water production from a solar water distillation device. They concluded that present evaporation and condensation models are the most reliable tool for predicting the daily production of water. Murugavela et al. (2013) reviewed different methods to improve the effectiveness of the inclined solar still by different researchers and compare their performance.

In this work, a computer simulation model for studying the unsteady-state thermal performance of a single tilted solar powered still which takes into account the thermal capacitance of the still is presented. The energy balance equations of an element along the solar still are formulated and solved simultaneously using the numerical method of Runge–Kutta. In addition, A comparative study between the computer simulation results and the experimental data obtained was carried out under the same conditions for validation.

Experimental system and procedure

Experimental rig setup

The experimental system as shown schematically in Fig. 1 has been used to provide comparison and validation for the mathematical model employed.

The absorber of the proposed single tilted solar basin is manufactured from steel sheet of 1.25 mm thickness, 100 cm length, and 50 cm width. The depth of the solar still is 10 cm. The absorber was painted with matt-finish black to enhance its absorptivity of sun radiation and was placed towards the south and tilted 20° to the horizontal, which provided an almost uniform thickness of a thin layer of water flow. Also, the tilted angle 20° towards the south is optimum for solar radiation as reported by Reindel et al. (1990) and Perez et al. (1990), respectively. The cover was clear glass of 6 mm thickness. The casing to the absorber was made of 1 mm thick galvanized iron and of slightly larger size, thus allowing fiber-glass insulation to be placed at the sides (25 mm thick) and backside of the absorber (50 mm thick). The glass cover was sealed to the casing using a weather strip and silicone rubber all around.

The absorber was fed by a constant head water tank that uses a float. The water was sprinkled uniformly at the top side of the absorber using galvanized pipe of ½ inch in diameter with 25 drilled holes each of 1 mm diameter. The spacing between any two successive holes was 20 mm, thus producing a nearly uniform film flow of water sliding down over the absorber plate. The flow of brine water was regulated by a calibrated valve placed between the water tank and the water pipe distributor in the absorber. The distilled water produced was collected by a half cylinder shaped steel sheet located at the underneath lower end of the glass cover, after which the distilled water is collected in vessels.

The entire system was supported and mounted on a base framework made of angle iron bars. The whole system could be adjusted manually and be set at any inclination angle. The various system temperatures were measured using calibrated type K-type thermocouples inserted at many locations in the system. Three thermocouples were placed at the absorber surface, two on the inside of the glass cover, one on the outside of the cover, and others to measure the water inlet, outlet, and distilled temperatures. A pyranometer was used to record the global incident insolation, which was fixed to a small base at one side of the casing at the same absorber inclination angle.

Experimental procedure

Experimental measurements were carried out as follows:

1. Measurements of total sun insolation at various temperatures every hour per day for a number of days at four different flow rates of water. These flow rates were 0.288, 0.348, 1.164, and 2.280 kg/h. The temperature of the water in the small water tank was taken as the temperature of the ambient at start, and the high irradiation during the testing days produced distilled water as indicated in the experimental results.
2. The amounts of the distilled water and the saline water were also taken hourly during the course of the experiment. The waste brine water is flushed out as often as necessary, then collected in vessels and removed away. It should be noted here that an accurate valve was used to regulate the flow of brine water through the solar still at a fixed rate for the whole day time of the experimental run. The valve was calibrated in situ and was kept under constant head during the time of the experiment.

System simulation

The present analysis represents models of the governing equations of the inclined single solar basin still by formulating both the temperature of the water flow and that of the absorber as functions of two independent parameters: the space coordinate along the axial distance for the brine water flow in the still as the first independent parameter and, the time as the second. Furthermore, the solar still was divided into axial elements with the assumption of linear variation of the temperature of the water flow, the cover, and the absorber along the element. In this way, only the time was kept as a single independent variable for each axial element, and the lumped model was employed for each element, which led to a coupled system of differential equations. Lumped models are frequently applied for analysis purposes in solar systems; Edenburn (1976), Garld and Kuehn (1989) and Ammari and Nimir (2003).

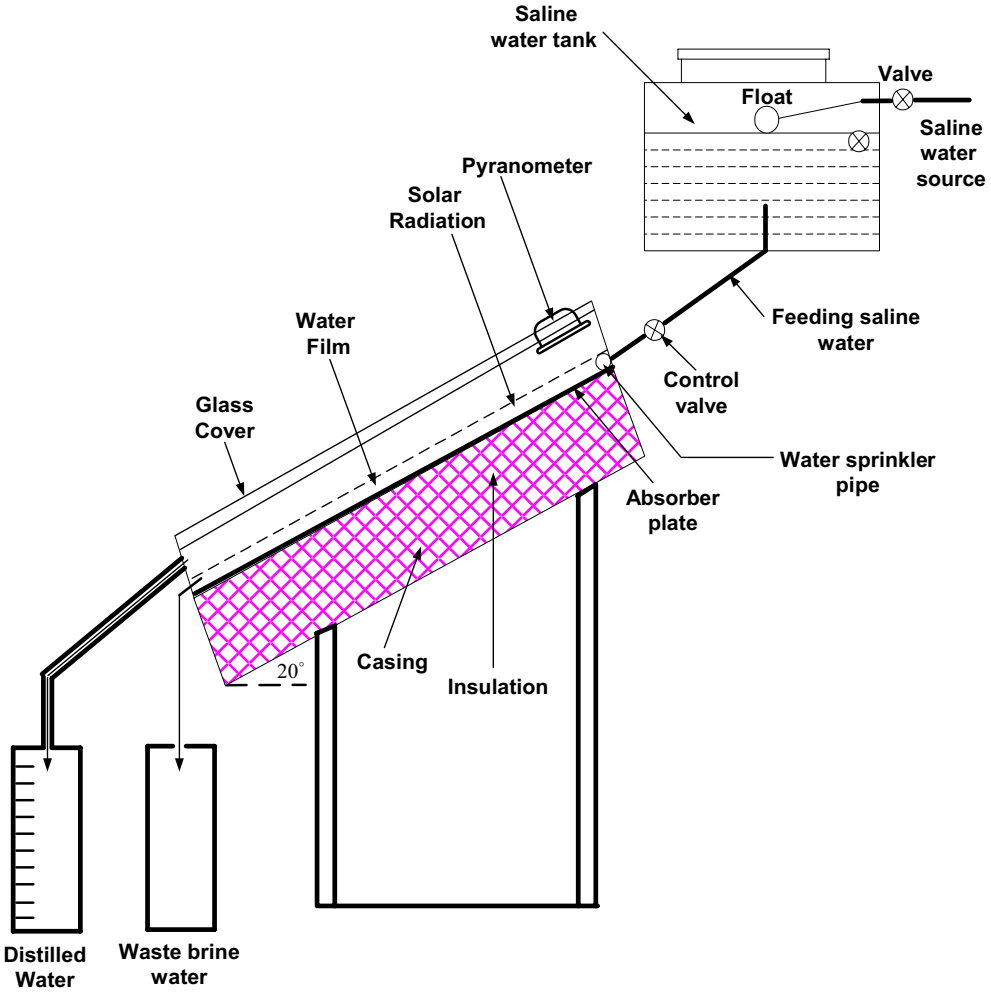

Fig. 1 Schematic diagram of tilted solar still experimental setup

The resulting system of differential equations was, therefore, solved simultaneously and computationally using Butcher's Runge–Kutta method of the fifth order, Chapra and Canale (1990). The temperature of each of the water flow, the glass cover, and the absorber elements as functions of the axial direction and time were predicted. In addition, the performance of the solar still was evaluated by computing the system efficiency over the period of a day. The inclined single solar basin still was computationally divided into a number of elements along the axial fluid flow direction. Each element was fragmented into three parts: the absorber plate, the brine water flowing over the absorber, and the glass cover as shown in Fig. 2. The energy balance equation was then applied simultaneously to each of the three parts of the elements. The solar absorption and energy transfer mechanisms are also shown in Fig. 2. The inclined single solar basin still was fully simulated as in the experimental setup. The simulation takes into account the position of the system to the south and inclined at an angle of 20°.

Governing equations

The energy conservation equation is applied simultaneously to each of the three parts of an element, glass cover, absorber plate and saline water, taking into consideration the unsteady-state thermal performance of each part (Ammari and Nimir 2003). Three separate control volumes are considered in the analysis of an element of the solar still: the glass cover, the absorber plate and part of the insulation, and the saline water as shown in Fig. 2. However, the following assumptions as reported by Shanmugan (2014) are considered for the energy balance equations of glass cover, absorber plate, and saline water:

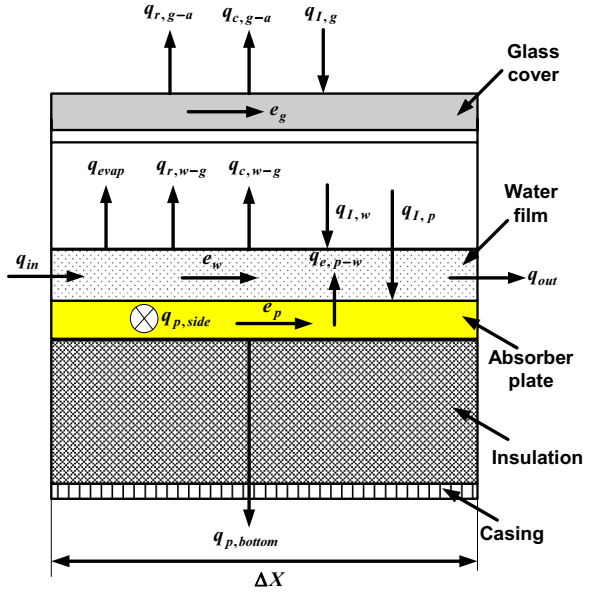

Fig. 2 Energy transfer on an element of the solar still

- There is no vapor leakage in solar still.
- It is an air tight basin and hence no heat loss.
- There is no temperature gradient across the basin water and glass cover of solar still.
- Water level inside the basin maintained at constant level.
- The governing heat transfer coefficients in the still are temperature-dependent.

Considering an element of length Δx and width W, the energy balance equation for the control volume of the glass cover is

$$q_{I,g} + q_{c,w-g} + q_{r,w-g} + q_{evap} = q_{c,g-a} + q_{r,g-a} + \frac{\partial e_g}{\partial t}, \tag{1}$$

where

$$q_{I,g} = I(t)A(1-\beta_g)\alpha_g : \text{ heat transfer by radiation from ambient air to glass cover} \tag{2a}$$

$$q_{c,w-g} = Ah_{c,w-g}((T_w(x,t) - T_g(x,t)) : \text{ heat transfer by convection from water to glass cover} \tag{2b}$$

$$q_{r,w-g} = Ah_{r,w-g}\big((T_w(x,t) - T_g(x,t)\big) : \text{ heat transfer by radiation from water to glass cover} \tag{2c}$$

$$q_{\text{evap}} = Ah_{\text{evap}}\big((T_w(x,t) - T_g(x,t)\big) : \text{ heat transfer of evaporation} \tag{2d}$$

$$q_{c,g-a} = Ah_{c,g-a}\big((T_g(x,t) - T_a(x,t)\big) : \text{ heat transfer by convection from glass cover to ambient air} \tag{2e}$$

$$q_{r,g-a} = Ah_{r,g-a}\big((T_g(x,t) - T_{\text{sky}}(x,t)\big) : \text{ heat transfer by radiation from glass cover to ambient air} \tag{2f}$$

$$\frac{\partial e_g}{\partial t} = \rho_g \text{Cp}_g V_g \left(\frac{\partial T_g(x,t)}{\partial t}\right) : \text{ rate of energy change of glass cover} \tag{2g}$$

By substitution of Eqs. (2a–2g) into Eq. (1) and rearrangement of parameters, the following differential equation is obtained for the temperature of the glass cover element:

$$\frac{\partial T_g(x,t)}{\partial t} = \frac{A}{\rho_g Cp_g V_g} \left[\begin{array}{l} I(t)\left(1-\beta_g\right)\alpha_g + \left(h_{c,w-g} + h_{r,w-g} + h_{evap}\right)\left(T_w(x,t) - T_g(x,t)\right) \\ - h_{c,g-a}\left(T_g(x,t) - T_a(t)\right) - h_{r,g-a}\left(T_g(x,t) - T_{sky}(t)\right) \end{array}\right] \tag{3}$$

The energy balance equation for the absorber plate and part of the insulation is

$$q_{I,p} = q_{c,p-w} + q_{p,\text{loss}} + \frac{\partial e_p}{\partial t}, \tag{4}$$

where

$$q_{I,p} = I(t)A\,\tau_g\tau_w\,\alpha_p : \text{ heat transfer by radiation to absorber plate} \tag{5a}$$

$$q_{c,p-w} = Ah_{c,p-w}\big((T_p(x,t) - T_w(x,t)\big) : \text{ heat transfer by convection from absorber plate to water} \tag{5b}$$

$$q_{p,\text{loss}} = q_{p,\text{bottom}} + q_{p,\text{side}} : \text{ heat loss from the absorber plate} \tag{5c}$$

$$q_{p,\text{bottom}} = A\big[T_p(x,t) - T_a(x,t)\big]/R_{b,\text{total}} : \text{ heat transfer from the bottom of the absorber to air} \tag{5d}$$

$$R_{b,\text{total}} = R_{b,\text{insulation}} + R_{b,\text{casing}} + R_{b,\text{convection}} \tag{5e}$$

$$q_{p,\text{side}} = A_s\big[T_p(x,t) - T_a(x,t)\big]/R_{s,\text{total}} : \text{ heat transfer from the side of the absorber to air} \tag{5f}$$

$$R_{s,\text{total}} = R_{s,\text{insulation}} + R_{s,\text{casing}} + R_{s,\text{convection}} : \text{ total thermal resistance} \tag{5g}$$

$$\frac{\partial e_p}{\partial t} = \left(\rho_p Cp_p V_p + r\rho_i Cp_i V_i\right)\left(\frac{\partial T_p(x,t)}{\partial t}\right) : \text{ rate of energy change of the absorber plate} \tag{5h}$$

And, r represents the percentage of the insulation layer attached to the absorber plate assumed to have the same temperature as the plate.

Substituting Eqs. (5a–5h) into Eq. (4) and rearranging the parameters yields the following differential equation for the temperature of the absorber plate, pipe and insulation part of the element,

$$\frac{\partial T_p(x,t)}{\partial t} = \frac{1}{\rho_p Cp_p V_p + r\rho_i Cp_i V_i} \left[\begin{array}{l} AI(t)\,\alpha_p \tau_g - Ah_{c,p-w}\big(T_p(x,t) - T_w(x,t)\big) \\ -\left(\dfrac{A}{R_{b,\text{total}}} + \dfrac{A_s}{R_{s,\text{total}}}\right)\big(T_p(x,t) - T_a(t)\big) \end{array} \right] \tag{6}$$

The energy balance equation for the part of the element of brine water film flowing over the absorber plate is

$$q_{I,w} + q_{c,p-w} + q_{in} = q_{c,w-g} + q_{r,w-g} + q_{\text{evap}} + q_{\text{out}} + \frac{\partial e_w}{\partial t}, \tag{7}$$

where

$$q_{I,w} = I(t)A\,\tau_g\,\alpha_w \ : \text{ heat transfer by radiation to water film} \tag{8a}$$

$$q_{c,p-w} = Ah_{c,p-w}\big((T_p(x,t) - T_w(x,t)\big) \ : \text{ heat transfer by convection from absorber to water film} \tag{8b}$$

$$q_{\text{in}} = \dot{m}_w C_{pw} T_{w,i}(x,t) \ : \text{ heat in the water film element of tilted solar still.} \tag{8c}$$

$$q_{c,w-g} = Ah_{r,w-g}\big((T_w(x,t) - T_g(x,t)\big) \ : \text{ heat transfer by radiation from water to glass cover} \tag{8d}$$

$$q_{r,w-g} = Ah_{r,w-g}\big((T_w(x,t) - T_g(x,t)\big) \ : \text{ heat transfer by radiation from water to glass cover} \tag{8e}$$

$$q_{\text{evap}} = Ah_{\text{evap}}\big((T_w(x,t) - T_g(x,t)\big) \ : \text{ heat transfer of evaporation} \tag{8f}$$

$$q_{\text{out}} = (\dot{m}_w - \dot{m}_c)C_{pw} T_{w,o}(x,t) \ : \text{ heat out from the water film element of the tilted solar still.} \tag{8g}$$

$$\frac{\partial e_w}{\partial t} = \rho_w Cp_w V_w \left(\frac{\partial T_w(x,t)}{\partial t}\right) \ : \text{ rate of energy change of water film} \tag{8h}$$

The implemented lumped model assumes linear temperature distribution across the fluid element, that is,

$$T_w(x,t) = \frac{1}{2}[T_{w,i}(x,t) + T_{w,o}(x,t)],$$

$$\text{and} \quad \frac{\partial T_w(x,t)}{\partial t} \cong \frac{\partial T_{w,o}(x,t)}{\partial t}$$

These two assumptions are assumed viable for the brine water element, which is too short in length, regardless of the length of the absorber.

Therefore, the differential equation for the temperature of the brine water element becomes

$$\frac{\partial T_{w,0}(x,t)}{\partial t} = \frac{1}{\rho_w Cp_w V_w} \left[\begin{array}{l} I(t)\,A\,(1-\rho_g - \cdots) + Ah_{c,p-w}\left(T_p(x,t) - \frac{1}{2}\big(T_{w,i}(x,t) + T_{w,0}(x,t)\big)\right) \\ -A\left(h_{c,w-g} + h_{r,w-g} + h_{evap}\right)\left(\frac{1}{2}\big(T_{w,i}(x,t) + T_{w,0}(x,t)\big) - T_g(x,t)\right) \\ +\dot{m}_w Cp_w\big(T_{w,i}(x,t) - T_{w,0}(x,t)\big) - \dot{m}_c Cp_w T_{w,0}(x,t) \end{array} \right] \tag{9}$$

Note that

$$A = W\Delta x$$
$$V_w = \delta W \Delta x,$$

where δ is the thickness of the brine water film layer over the absorber plate, which was assumed based on the experimental observations, and it was on average around 0.1 mm.

The condensation rate $\dot{m}_c$ is obtained by

$$\dot{m}_c = \frac{q_{\text{evap}}}{h_{fg}} = \frac{Ah_{\text{evap}}\big(T_w(x,t) - T_g(x,t)\big)}{h_{fg}} \tag{10}$$

The performance of a solar basin still could be evaluated by calculating its efficiency, $\eta(t)$, as

$$\eta(t) = \frac{q_{\text{evap}}}{I(t)A} \tag{11}$$

The correlations employed to estimate the convection heat transfer coefficients, $h_{c,w-g}$, $h_{c,g-a}$, and $h_{c,p-w}$, the radiation heat transfer coefficients, $h_{r,w-g}$ and $h_{r,g-a}$, and the evaporating heat transfer coefficient h_{evap} are given in "Appendix". In the simulation process, the axial direction was for $0 \le x \le L$, where L is the solar still total length, and the time was 12 h from sunrise to the sunset, 6 a.m. $\le t \le$ 6 p.m.

Simulation method

Boundary and initial conditions

The temperatures of the glass cover, the absorber plate, and the water elements were solved based on the boundary and initial conditions, which were the functions of the flow in the axial direction, x, and the time, t. The initial conditions at $x = 0$ to L for the main solar still components were taken as follows; for the glass cover $T_g(x,0) = T_a(0)$, for the absorber plate, $T_p(x,0) = T_a(0)$ and the water inlet and outlet of solution; $T_{w,i}\,(x,0) = T_{w,o}(x,0) = T_a(0)$. Also, the boundary conditions at $t = 0$ to 12 h for the same components were taken as follows for the glass

cover; $T_g(0,t) = T_a(t)$, for the absorber cylinder; $T_p(0,t) = T_a(t)$, and the water inlet and outlet $T_{w,i}(0,t) = T_a(t)$.

Solution method

Runge–Kutta method of the fifth order was used to solve simultaneously and numerically the governing equations for the temperatures of the glass cover, the absorber plate, and the water flow elements for the solar still. The outlet water temperature of the elements was attained by the numerical solution of Eq. (9) according to Runge–Kutta method of the fifth order as follows:

$$T_{w,0}(i,j+1) = T_{w,0}(i,j) + \frac{\Delta t}{90}(\text{HTML translation failed}) [7k1_w + 32k3_w + 12k4_w + 32k5_w + 7k6_w], \quad (12)$$

where

$$k1_w = f_w\left[t(j), T_{w,0}(i,j)\right]$$

$$k2_w = f_w\left[t(j) + \frac{\Delta t}{4}, T_{w,0}(i,j) + \frac{\Delta t}{4}k1_w\right]$$

$$k3_w = f_w\left[t(j) + \frac{\Delta t}{4}, T_{w,0}(i,j) + \frac{\Delta t}{8}k1_w + \frac{\Delta t}{8}k2_w\right]$$

$$k4_w = f_w\left[t(j) + \frac{\Delta t}{2}, T_{w,0}(i,j) - \frac{\Delta t}{2}k2_w + \Delta t k3_w\right]$$

$$k5_w = f_w\left[t(j) + \frac{3\Delta t}{4}, T_{w,0}(i,j) + \frac{3\Delta t}{16}k1_w + \frac{9\Delta t}{16}k4_w\right]$$

$$k6_w = f_w\left[t(j) + \Delta t, T_{w,0}(i,j) - \frac{3\Delta t}{7}k1_w + \frac{2\Delta t}{7}k2_w + \frac{12\Delta t}{7}k3_w - \frac{12\Delta t}{7}k4_w + \frac{8\Delta t}{7}k5_w\right]$$

and $f_w(t, T_{w,0})_{i,j} =$ the right hand side of Eq. (9).

$x(i) = i\Delta x, \quad i = 1, 2, 3, \ldots, N_i,$
where $Ni = L/\Delta x$, with $\Delta x = 10$ mm

$t(j) = j\Delta t, \quad j = 1, 2, 3, \ldots, N_j,$
where $N_j =$ total time$/\Delta t$, with $\Delta t = 10\,s$,

Similar numerical solution of Eqs. (3) and (6) was employed to compute the time-dependent temperature distribution along the glass cover and the absorber plate parts of the elements, respectively, using the fifth-order of Runge–Kutta method.

Procedure

Polynomial relations of the variation in the water and air thermophysical properties with temperature were accounted for using these properties as functions of temperature (Kreith and Bohn 1993). The temperatures used were mean temperature of water element, absorber-water temperature, absorber-ambient air temperature, glass-water temperature, and glass-ambient air temperature. Furthermore, the water flow type over the absorber plate, laminar or turbulent, was evaluated for each flow rate considered since the heat transfer coefficient is very sensitive to the regime. The present computational procedure was, therefore, based on the water flow, and it was iterative since the temperatures and consequently the heat transfer coefficients were recalculated during a time step. The simulation program was written in Fortran, and the time increment used, Δt, was as small as one second.

Results and discussion

The thermal performance of the tilted solar water basin at unsteady conditions was investigated. A comparison of the simulation results with the experimental measurements was initially made to verify the modeling used. In the modeling, convergence of solutions was achieved. The model incorporated the following assumptions:

- Uniform temperature distribution across any element.
- Uniform brine water flow at the inlet and downstream over the whole of the absorber.
- Uniform distilled water layer over the whole underneath area of the glass cover.
- Design parameters of typical solar water stills were considered.

The measured global radiation during the course of the experiments of 4 days is depicted in Fig. 3. Maximum daily measured irradiation values of 1240, 1050, 1175, and 970 W/m^2 were obtained during the following days: 11, 12, 13, and 14 of April, 2007, respectively. The global radiation trends were also used in the numerical solution.

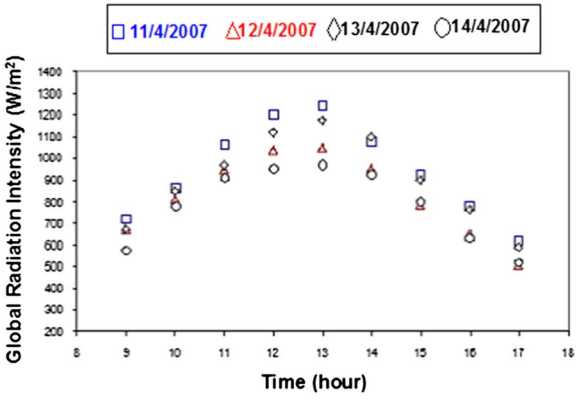

Fig. 3 Measured global radiation intensity

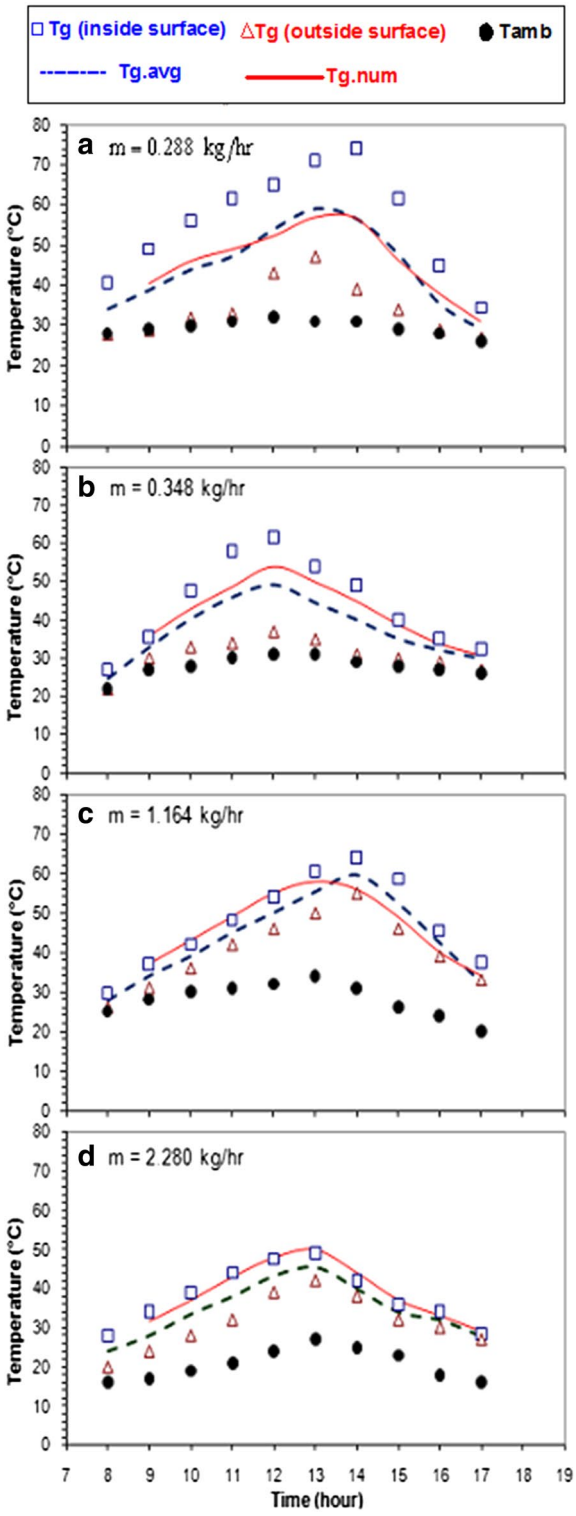

Fig. 4 Comparison between experimental and numerical glass cover temperatures with time for different measured ambient temperatures at different mass flow rate of water flow. **a** m = 0.288 kg/h, **b** m = 0.348, **c** m = 1.164, **d** m = 2.280

Also, solar radiation intensity is found to be the maximum at noon and then decreases gradually till 5 pm.

A comparison between the experimental data and the analytical results for the average temperature of the glass cover is presented in Fig. 4a–d. The temperature results were for four different mass flow rates of water of 0.288, 0.348, 1.164, and 2.280 kg/h and with measured radiation intensity during the days of running the experiments 11, 12, 13, and 14 of April, 2007, respectively. Also, Fig. 4 includes the ambient air temperature during the days of conducting the experiments.

It is clear from Fig. 4 that all the measured and computed glass cover average temperature trends as well as the ambient are similar in that they gradually start to increase in the morning with the increased radiation intensity, reaching a maximum early afternoon due to the thermal capacity of the system and decreasing slightly in the afternoon as the radiation drops off till 5.00 p.m. The predicted glass cover average temperature matched the corresponding experimental measurements reasonably closely, with best agreement at $\dot{m}$ of 0.288 kg/h. It should be noted here that the temperature $T_{g,\text{inside}}$ for a mass flow rate $\dot{m}$ of 0.288 is higher than the other days because the hourly measured irradiation values (8.00 a. m. to 5.00 p.m.) during the day 11 of April 2007 is the highest compared with the other days 12, 13, and 14th of April 2007. Consequently, the temperatures of $T_{g,\text{inside}}$ and $T_{g,\text{outside}}$ of the glass cover would be higher on 11 April (Fig. 4a). Furthermore, it is observed that that the difference in temperature between $T_{g,\text{inside}}$ and $T_{g,\text{outside}}$ shown in Fig. 4a is the highest compared with that of other days. This can be attributed to the higher values of hourly measured irradiation on the 11th of April compared with the other days, and to the lowest mass flow rate of brine water.

Figure 5a, b shows the numerical and experimental results of the absorber plate temperatures variation with time for different mass flow rate of water flow and ambient temperatures. It can be observed that the temperature trends of the absorber plate temperature are the same, although the numerical results over predicted the systematic experimental measurements most of the day for the three higher mass flow rate of water flow (0.348, 1.164, 2.280) kg/h with a maximum difference of about 17 %, except at the lowest water mass flow rate of 0.288 kg/h.

A comparison between the experimental and the numerical results for the distilled water produced is displayed in Fig. 6a, b. The investigation was conducted under the measured conditions of solar irradiation and ambient temperatures of the 11th, 12th, 13th, and 14th days of April 2007, corresponding to the mass flow rates of brine water considered. The comparison covers the variation of distillate water produced with day time. It can be seen that the distillate produced starts almost at the same early hours of the

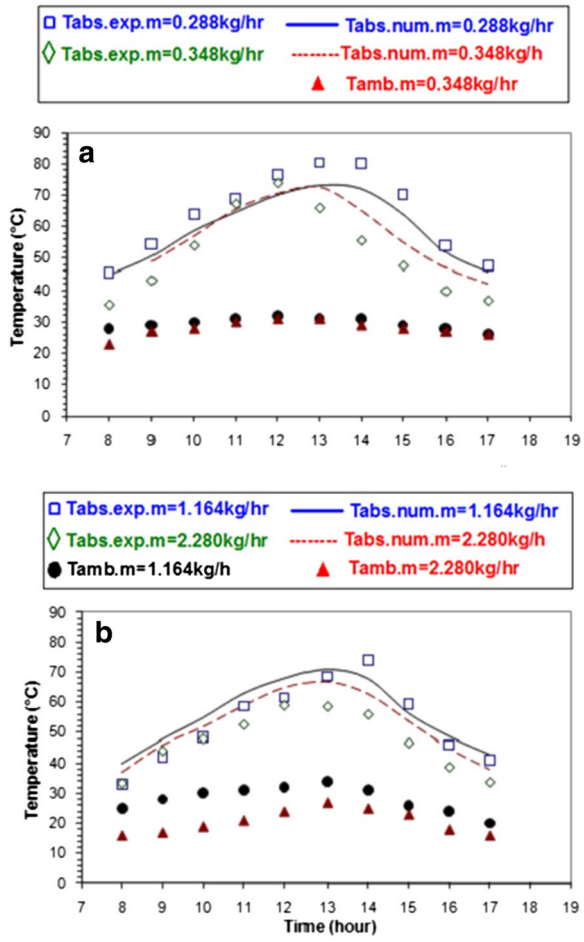

Fig. 5 Comparison between experimental and numerical absorber temperatures with time for different measured ambient temperatures at different mass flow rate of water flow. **a** m = 0.288 kg/h and m = 0.348, **b** m = 1.164 and m = 2.280

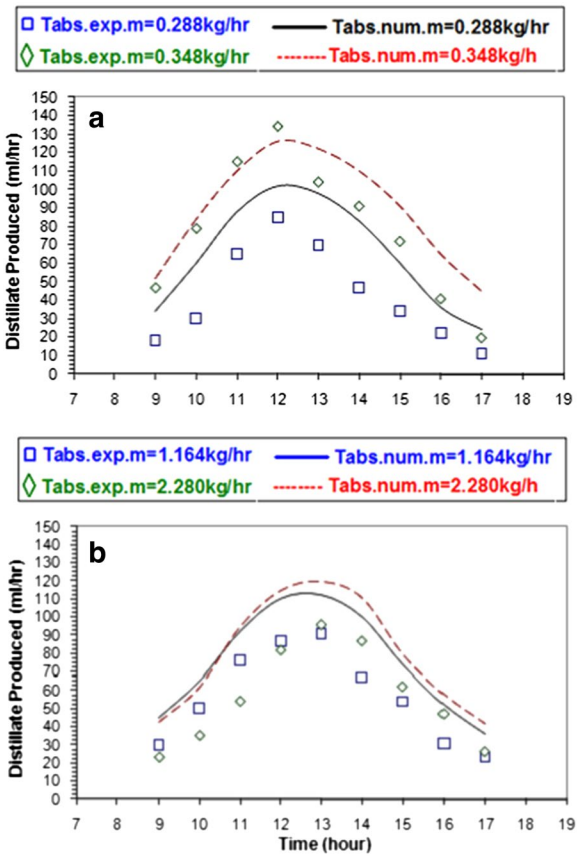

Fig. 6 Comparison between experimental and numerical distilled water production variation with time at different mass flow rate of water flow. **a** m = 0.288 kg/h and m = 0.348, **b** m = 1.164 and m = 2.280

morning and starts to increase with increased irradiation. As the time approached mid day, higher values particularly at the low water mass flow rate of $\dot{m} = 0.348$ kg/ h 0.384 are observed, But as the day proceeded, the distillate production decreased gradually. This behavior was observed regardless of the water mass flow rate within the range tested. In general, similar trends and behaviour during the whole day were noticed, although the increase in the distillate production of the numerical results reveals discrepancies in comparison with the predicted experimental results, and in particular, around mid day, the differences were more substantial. It is observed that the experimental distilled water production (m = 0.348 kg/h) is higher than that in the other days. This is can be attributed to the hourly irradiance values and lower heat transfer losses on that day.

The daily total distillate collected over the course of measurements, in addition to these computed, is shown in Table 1. The total difference percentage is due to the fact that it represents the summation of differences over the whole day. The largest difference in total daily distillate produced can be seen at the lowest water mass flow rate as the brine water over the absorber had more time to absorb heat from the rapidly absorbed irradiation by the absorber.

The variation of the water distillate with mass flow rate for both types of results is noticed. However, the effect of the mass flow rate of brine water on the distillate produced at some global radiation is shown in Fig. 7, whereas the distillate produced at global radiation of 950 W/m^2 (at around 11 a.m. for almost all mass flow rates of brine water) is examined. The figure indicates clearly that the best performance was obtained at $\dot{m}$ of 0.348 kg/h for both the experimental and numerical results.

Figure 8a, b shows the variation of the system's instantaneous efficiency with time for the experimental and numerical results. Both of the systematic and theoretical efficiency values were estimated using Eq. (11). The experimental

Table 1 Total daily distillate collected

Brine water mass flow rate (kg/h)	Maximum global radiation (W/m^2)	Daily total distillate (experimental) (ml/day)	Daily total distillate (numerical) (ml/day)	Total difference percentage (%)
0.288	970	475	568	+19.5
0.348	1175	710	805	+13.3
1.164	1050	595	686	+15.3
2.280	1240	620	726	+17.1

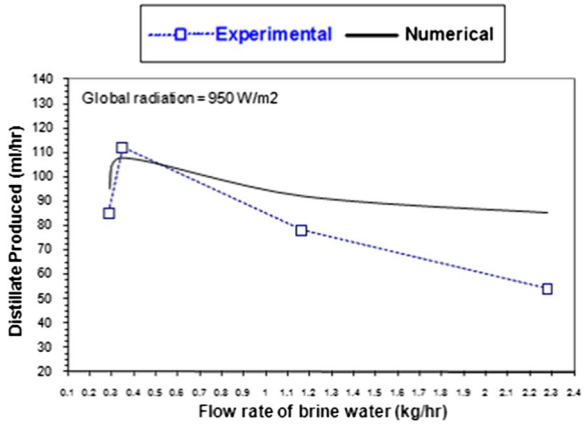

Fig. 7 Comparison between experimental and numerical distilled water production against brine water mass flow rate

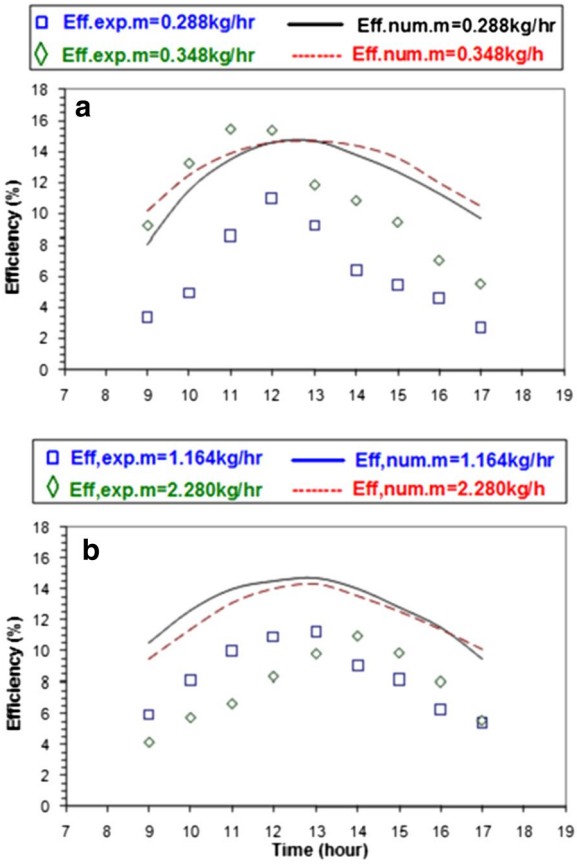

Fig. 8 Comparison between experimental and numerical efficiencies variation with time at different mass flow rate of water flow. **a** m = 0.288 kg/h and m = 0.348 **b** m = 1.164 and m = 2.280

instantaneous efficiencies were within the range of 3.5–15.5 %. It can be seen from Fig. 8a, b that the predicted efficiencies over the whole day and for all brine water mass flow rates are seen to be substantially higher than the corresponding experimental efficiencies, except for the mass flow rate of 0.348 kg/h around midday (i.e. between the hours 10.00 a.m. and 12.00 a.m.). On the other hand, the simulated efficiencies are seen to be somewhat flatter for all water mass flow rates although they have a peak around mid day, ranging between 8 and 15 %. In general, the agreement between both efficiencies, numerical and experimental, was reasonable, taking into consideration the assumptions incorporated into the mathematical model and the accuracy of measurements. The results of the current work agree well with similar work found in the open literature (Badusha and Arjunan 2013).

Error analysis

The errors that occurred in measuring instruments are shown in Table 2. The errors were calculated for thermocouples, pyranometer, anemometer, thermometer, and measuring jar. The minimum error that occurred in any instrument is equal to the ratio between its least count and minimum value of the output measured. To estimate the uncertainties in the results presented in this work, the approach described by Barford (1990) is applied. The uncertainty in the measurements is defined as the root sum square of the fixed error of the instrumentation and the random error observed during different measurements.

Table 2 Accuracies and ranges of measuring instruments

No.	Instrument	Accuracy	Range	% Error
1	Thermocouple	±1 °C	0–100 °C	0.25
2	Thermometer	±1 °C	0–100 °C	0.25
3	Kipp–Zonen Pyranometer	±1 W/m^2	0–5000 W/m^2	0.20
4	Anemometer	±0.1 m/s	0–15 m/s	4.0
5	Measuring jar	±10 ml	0–500 ml	10

Conclusions

It is known that the solar distillation exhibits considerable economic advantages over the other water distillation processes because it costs less, uses free energy, and reduces operating costs. Producing fresh water by a solar still with its simplicity would be a potential option to supply fresh water. In this work the unsteady-state thermal performance of tilted solar water still had been analyzed and predicted at various mass flow rates. The mathematical model was investigated to check the feasibility of employing such models in tilted solar water stills. The different modes of heat transfer of the still were modeled and numerical solution for the time-dependent governing equations was performed using Runge-Kutta method of the 5th order. Comparison between the numerical and experimental results was made. The results have provided the following findings:

1. The generally satisfactory agreement between the theoretical and experimental results indicate that the present mathematical model is feasible for solving the unsteady-solar water tilted stills, and can be used for preliminary design purposes to predict the influence of various pertinent parameters (radiation intensity, properties of glass cover, properties of absorber, ambient temperature, temperatures of the glass cover, the absorber plate, and the water flow solar still size, Heat transfer coefficients, and mass flow rate on the thermal performance of solar water tilted stills.
2. The distillate water produced was noticeably larger at the water mass flow rate of 0.348 kg/h than the other flow rates considered during most of the day. The system used was small in size, 0.5 m^2 exposure area, and for practical domestic applications one would need much larger exposure area. However, the whole purpose of this work was to check the success of the simulation model to analyze tilted solar water basins.
3. Optimization of the design parameters is possible with the thermal model proposed and can be used for large-scale installations
4. The correlations used in this work can be generalized for all types of solar stills
5. The best performance was obtained at $\dot{m}$ of 0.348 kg/h for both the experimental and numerical results.
6. In general, the agreement between both efficiencies, numerical and experimental, was reasonable, taking into consideration, the assumptions incorporated into the mathematical model and the accuracy of measurements. However, the simulated efficiencies are ranging between 8 and 15, while experimental instantaneous efficiencies were within the range of 3.5–15.5 %.

Nomenclature

A	Area (m^2)
Cp	Specific heat (kJ/kg K)
e	Energy (kJ)
h	Convection heat transfer coefficient (W/m^2 K)
h_{fg}	Latent heat of vaporization (kJ/kg)
I	Irradiation (W/m^2)
k	Thermal conductivity (W/m K)
$k1$–$k5$	Runge–Kutta factors
L	Still length (m)
$\dot{m}$	Mass flow rate (kg/s)
N_i	Number of elements
N_j	Number of time steps
Nu	Nusselt number
P	Pressure (Pa)
Pr	Prandtl number
q	Heat transfer (kW)
R	Thermal resistance (m^2 K/W)
Re	Reynolds number
T	Temperature (°C)
t	Time (s)
V	Volume (m^3)
v	Velocity (m/s)
W	Still width (m)
x	Axial distance measured from inlet of brine water over the absorber (m)

Greek

α	Absorptivity
β	Reflectivity
δ	Thickness of brine water layer
Δx	Element length (m)
Δt	Time step (s)
ε	Emissivity
η	Efficiency
μ	Viscosity (kg/m s)
ρ	Density (kg/m^3)
σ	Stefan–Boltzman constant $= 5.67 \times 10^{-8}$ ($W/m^2 K^4$)
τ	Tranmissivity

Subscript

a	Air
b	Bottom
c	Convection heat transfer, or condensate
evap	Evaporation

g	Glass
I	Radiation
i	Insulation
p	Absorber plate
r	Radiation heat transfer
s	Side
w	Water
w,i	Water inlet
w,o	Water outlet

Authors' contributions
ME carried out the design, modelling and experimental work, participated in analysing the results and discussion and drafted the manuscript. HA participated in the design of the study and performed the simulation procedure, contributed to the discussion and helped to draft the manuscript. Both authors read and approved the final manuscript.

Author details
[1] Mechanical Engineering Department, Philadelphia University, Amman, Jordan. [2] Mechanical Engineering Department, Mutah University, Karak, Jordan.

Competing interests
The authors declare that they have no competing interests.

Appendix

The different heat transfer coefficients for each surface and fluid in the simulation program were evaluated (Note that the temperature T in the equations is in Kelvin) as follows:

Radiation heat transfer coefficient from top of glass cover surface

The radiation heat transfer coefficient from the top glass cover to the sky referred to the ambient temperature is

$$h_{r,g-a} = \sigma \varepsilon_g \left(T_g + T_{\text{sky}}\right)\left(T_g^2 + T_{\text{sky}}^2\right)\frac{\left(T_g - T_{\text{sky}}\right)}{\left(T_g - T_a\right)},$$

whereas $T_{\text{sky}} =$ is the sky temperature (Khalifa and Hamood 2009) $= 0.0552 T_a^{1.5}$

Radiation heat transfer coefficient between brine water and glass cover

The radiation heat transfer coefficient between the brine water and the glass cover, $h_{r,w-g}$, is computed as follows:

$$h_{r,w-g} = \frac{\sigma\left(T_w^2 + T_g^2\right)\left(T_w + T_g\right)}{\frac{1}{\varepsilon_w} + \frac{1}{\varepsilon_g} - 1}$$

Convection heat transfer coefficient from the glass cover due to wind

The convection heat transfer coefficient from the top of glass cover due to wind, $h_{c,g-a}$, is correlated by Watmuff et al. (1977) as

$h_{c,g-a} = 2.8 + 3.3\, v_{\text{wind}}$,

whereas v_{wind} is the wind velocity at the site of the experimental setup, measured as 2.0 m/s.

Convection heat transfer coefficient between brine water and glass cover

The convection heat transfer coefficient, $h_{c,w\text{-}g}$, between the brine water and the glass cover is given by the following relationship:

$$h_{c,w-g} = 0.884\left[T_w - T_g + \frac{T_w\left(P_w - P_g\right)}{268.9 \times 10^3 - P_w}\right]^{\frac{1}{3}}$$

Evaporation heat transfer coefficient

The evaporation heat transfer coefficient is taken from the following correlation:

$$h_{\text{evap}} = 16.273 \times 10^{-3} h_{c,w-g}\frac{\left(P_w - P_g\right)}{\left(T_w - T_g\right)}$$

Convection heat transfer coefficient between brine water and absorber plate

It was assumed that the flow was hydrodynamically fully developed from the start of water flow on the absorber plate in the code. Therefore, the convective heat transfer coefficient between the brine water and the absorber plate, $h_{c,p-w}$, was modeled according to the flow regime, laminar or turbulent. Thus, Reynolds number ($\text{Re}_x = \rho_w v_w \cdot x/\mu_w$) was computed first so that if the flow was mainly laminar ($\text{Re}_x < 5 \times 10^5$), $h_{c,p-w}$ was evaluated from the fully developed laminar flow correlation:

$$\text{Nu}_x = h_{c,p-w}x/k = 0.332\,\text{Re}_x^{1/2}\,\text{Pr}^{1/3}$$

If the flow regime was turbulent, $h_{c,p\text{-}w}$ was obtained from the fully developed turbulent flow correlation,

$$\text{Nu}_x = h_{c,p-w}x/k = 0.0296\,\text{Re}_x^{1/2}\,\text{Pr}^{1/3},$$

where Pr = Prandtl number,

The fluid properties were evaluated at the mean temperature of the fluid and surface.

Bottom and side thermal resistances

The convective heat transfer coefficients from the bottom and sides of the collector to the outside air were assumed small in comparison with the insulation thermal resistance. The insulation resistance was calculated by

$R_i =$ insulation thickness/insulation thermal conductivity.

Received: 6 August 2015 Accepted: 23 October 2015
Published online: 26 November 2015

References

Abdallah, S., Abu-Khader, M. M., & Badran, O. (2009). Effect of various absorbing materials on the thermal performance of solar stills. *Desalination, 242*, 128–137.

Abu-Arabi, M., Zurigat, Y., Al-Hinaib, H., & Al-Hiddabi, S. (2002). Modeling and performance analysis of a solar desalination unit with double-glass cover cooling. *Desalination, 143*, 173–182.

Abu-Hijleh, B. A. K., & Rababah, H. M. (2003). Experimental study of a solar still with sponge cubes in basin. *Energy Conversion and Management, 44*, 1411–1418.

Ahsan, A., Imteaz, M., Devd, R., & Arafate, H. A. (2013). Numerical models of solar distillation device: Present and previous. *Desalination, 311*, 173–181.

Ahsan, A., Imteaz, M., Rahman, A., Yusuf, B., & Fukuhara, T. (2012). Design, fabricate and performance analysis of an improved solar still. *Desalination, 292*(2012), 105–112.

Akash, B. A., Mohsen, M. S., & Nayfeh, W. (2000). Experimental study of the basin type solar still under local climate conditions. *Energy Conversion and Management, 41*, 883–890.

Alaudeen, A., Johnson, K., Ganasundar, P., Syed Abuthahir, A., Srithar, K. 2014. Study on stepped type basin in a solar still. *Journal of King Saud University-Engineering Sciences*, *26*(2), 176–183. http://www.sciencedirect.com/science/article/pii/S1018363913000172-item.

Al-Hayeka, I., & Badran, O. O. (2004). The effect of using different designs of solar stills on water distillation. *Desalination, 169*(2), 121–127.

Ammari, H. D., & Nimir, Y. L. (2003). Experimental and theoretical evaluation of the performance of a tar solar water heater. *Energy Conversion and Management, 44*(19), 3037–3055.

Badran, A. A., & Al-Tahaineh, H. A. (2005). The effect of coupling a flat-plate collector on the solar still productivity. *Desalination, 183*, 137–142.

Badran, A. A., Assaf, K., Kayed, S., Ghaith, F. A., & Hammash, M. I. (2004). Simulation and experimental study for an inverted trickle solar still. *Desalination, 164*, 77–85.

Badusha, R., & Arjunan, T. V. (2013). Performance analysis of single slope solar still. *International Journal of Mechanical Engineering and Robotics Research, 2*(4), 74–81.

Bradford, N. C. (1990). *Experimental measurements: precision error and truth*. New York: Wiley.

Chapra, S. C., & Canale, R. P. (1990). *Numerical methods for engineers*. New York: McGraw-Hill.

Dev, R., & Tiwari, G. N. (2010). Characteristics equation of a hybrid (PV/T) active solar still. *Desalination, 254*(1–3), 126–137.

Duffie, J. A., & Beckman, W. A. (1991). *Solar engineering of thermal processes*. New York: John Wiley.

Edenburn, M. W. (1976). Performance analysis of cylindrical parabolic focusing collector and comparison with experimental results. *Solar Energy, 18*, 437–444.

Fath, H. E. S., & Hosny, H. M. (2002). Thermal performance of a single-sloped basin still with an inherent built-in additional condenser. *Desalination, 142*, 19–27.

Garld, E. W., & Kuehn, T. H. (1989). Performance analysis of a parabolic trough solar collector with porous absorber receiver. *Solar Energy, 42*, 281–292.

Janarthanan, B., Chandrasekaran, J., & Kumar, S. (2005). Evaporative heat loss and heat transfer for open- and closed-cycle systems of a floating tilted wick solar still. *Desalination, 180*, 291–305.

Kabeel, A. E., & El-Agouz, S. A. (2011). Review of researches and developments on solar stills. *Desalination, 276*(1–3), 1–12.

Kabeel, A. E., Khalil, A., Omara, Z. M., & Younes, M. M. (2012). Theoretical and experimental parametric study of modified stepped solar still. *Desalination, 289*, 12–20.

Kaushal, A. (2010). Varun, "Solar stills: A review". *Renewable and Sustainable Energy Reviews, 14*, 446–453.

Khalifa, A. N., & Hamood, A. M. (2009). Performance correlations for basin type solar stills. *Desalination, 249*(1), 24–28.

Tiwari, A. K., & Tiwari, G. N. (2007). Thermal modeling based on solar fraction and experimental study of the annual and seasonal performance of a single slope passive solar still: the effect of water depths. *Desalination, 207*, 184–204.

Kreith, F., & Bohn, M. S. (1993). *Principles of heat transfer*. St. Paul: West Publishing Co.

Kumar, S., Tiwari, G. N., & Gaur, M. K. (2010). Development of empirical relation to evaluate the heat transfer coefficients and fractional energy in basin type hybrid (PV/T) active solar still. *Desalination, 250*(1), 214–221.

Madhlopa, A., & Johnstone, C. (2009). Numerical study of a passive solar still with separate condenser. *Renewable Energy, 34*, 1668–1677.

Mahdi, J. T., Smith, B. E., & Sharif, A. O. (2011). An experimental wick type solar still system: design and construction. *Desalination, 267*(1–3), 233–238.

NASA surface meteorology and solar energy: Global data. power.larc.NASA.gov/cgi-bin/cgiwrap/solar/global.cgi? Accessed 5 September 2015 (**email: nasa.gov**).

Murugaval, K. K., & Srithar, K. (2011). Performance study on basin type double slope solar still with different wick materials and minimum mass of water. *Renewable Energy, 36*, 612–620.

Murugavela, K. K., Anburaja, P., Hansonb, R. S., & Elangoc, T. (2013). Progresses in inclined type solar stills. *Renewable and Sustainable Energy Reviews, 20*, 304–377.

Murugavela, K. K., Chockalingama, K. K. S. K., & Srithar, K. (2008). Progresses in improving the effectiveness of the single basin passive solar still. *Desalination, 220*, 677–686.

Naim, M. M., & Abd El Kwui, M. A. (2002). Non-conventional solar stills Part 1. Non-conventional solar stills with charcoal particles as absorber medium. *Desalination, 153*, 55–64.

Perez, R., Ineichen, P., & Seals, R. (1990). Modelling daylight availability and irradiance components from direct and global irradiance. *Solar Energy, 44*(5), 271–289.

Reindel, D. T., Beckman, W. A., & Duffi, J. A. (1990). Evaluation of hourly tilted surface radiation model. *Solar Energy, 45*(1), 9–17.

Sahoo, B. B., Sahoo, N., Mahanta, P., Borboraa, L., Kalitaa, P., & Saha, U. K. (2008). Performance assessment of a solar still using blackened surface and thermocol insulation. *Renewable Energy, 33*, 1703–1708.

Sampathkumar, K., Arjunan, T. V., Pitchandi, P., & Senthilkumar, P. (2010). Active solar distillation—a detailed review. *Renewable and Sustainable Energy Reviews, 14*, 1503–1526.

Shanmugan, S. (2014). Experimental analysis of a single slope single basin solar still with hot water provision. *International Journal of Applied and Natural Sciences, 3*(1), 19–24.

Shukla, S. K., & Sorayan, V. P. S. (2005). Thermal modeling of solar stills: an experimental validation. *Renewable Energy, 30*(5), 683–699.

Singh, H. N., & Tiwari, G. N. (2004). Monthly performance of passive and active solar stills for different Indian climatic conditions. *Desalination, 168*, 145–150.

St. Headley, C. (1973). Cascade solar still for distilled water production. *Solar Energy, 15*, 245–258.

Tabiriz, F. F., Dashtban, M., Moghaddam, H., & Razzaghi, K. (2010). Effect of water flow on internal heat and mass transfer and daily productivity of a weir type cascade solar still. *Desalination, 260*(1–3), 239–247.

Tabiriz, F. F., & Sharak, A. Z. (2010). Experimental study of an integrated basin solar still with a sandy heat reservoir. *Desalination, 253*(1–3), 195–199.

Tanaka, H., & Nakatake, Y. (2007). Improvement of the tilted wick solar still by using a flat plate reflector. *Desalination, 216*, 139–146.

Tanaka, H., & Nakatake, Y. (2009). Increase in distillate productivity by inclining the flat plate external reflector of a tilted-wick solar still in winter. *Solar Energy, 83*, 785–789.

Tiwari, G. N., Singh, H. N., & Tripathi, R. (2003). Present status of solar distillation. *Solar Energy, 75*(5), 367–373.

Tiwari, A. K., & Tiwari, G. N. (2006). Effect of water depths on heat and mass transfer in a passive solar still: in summer climatic condition. *Desalination, 195*, 78–94.

Tripathi, R., & Tiwari, G. N. (2004). Performance evaluation of a solar still by using the concept of solar fractionation. *Desalination, 169*(1), 69–80.

Velmurugan, V., & Srithar, K. (2011). Performance analysis of solar stills based on various factors affecting the productivity—a review. *Renewable and Sustainable Energy Reviews, 15*(2), 1294–1304.

Voropoulos, K., Mathioulakis, E., & Belessiotis, V. (2003). Analytical simulation of energy behavior of solar stills and experimental validation. *Desalination, 153*(1–3), 87–94.

Watmuff, J.H., Charters, W.W.S. & Proctor, D. 1977. Solar and wind induced external coefficients for solar collectors. COMPLES, (2), 56.

Xiao, G., Wang, X., Ni, M., Wang, F., Zhu, W., Luo, Z., & Cen, K. (2013). A review for solar stills for brine desalination. *Applied Energy, 103*, 642–652.